Time Resolved X-Ray Imaging of Dendritic Growth in Binary Alloys

R. H. Mathiesen,[1] L. Arnberg,[2] F. Mo,[1] T. Weitkamp,[3] and A. Snigirev[3]
[1]*Department of Physics, Norwegian University of Science and Technology, N-7491 Trondheim, Norway*
[2]*Department of Materials Technology, Norwegian University of Science and Technology, N-7491 Trondheim, Norway*
[3]*ESRF, Experiments Division, BP 220, F-38043 Grenoble cedex, France*
(Received 2 July 1999)

Direct beam x-ray imaging, with intense coherent monochromatic synchrotron radiation and a fast readout low noise detector has been used for *in situ* studies of cellular and dendritic solidification of Sn-Pb alloys. Temporal and spatial resolutions down to $\sim$0.7 s and $\sim$2.5 μm, respectively, with a field of view up to 1 mm^2 were obtained. The collected images display features from both phase and amplitude contrast which, combined with the attainable temporal resolution, provide a method with the potential to uncover dynamic processes in nonequilibrium solidification.

PACS numbers: 68.45.–v, 68.70.+w, 81.05.Bx, 81.30.Fb

In several types of nonequilibrium systems, propagating fronts between two phases appear as spatiotemporal structures at a macroscopic level. A common problem for such phenomena is to establish a consistent theory predicting the morphology of the interface as a function of its velocity field. The progress of a solid-liquid front during nonequilibrium crystal growth falls into this type of incompletely explained phenomena [1], of which traces can be observed in solidified alloys as dendritic microstructures. The microstructure has a strong influence on the mechanical properties of a solid [2,3], and therefore, a better understanding of growth processes and their dependence on various physicochemical parameters is of major importance in materials science as well. Self–consistent dendritic growth models exist which describe the propagation and curvature of an energetically anisotropic solid-liquid interface in the presence of capillarity effects [4]. Other effects, like interactions between adjacent interfacial features or solute diffusion, may give rise to more physical self-consistent models. Accordingly, experiments are required to evaluate the merits of such models and clarify the validity of underlying parametric assumptions [1].

In the last decade various numerical approaches [5] have been used to solve the nonlinear integro-differential equations satisfying the solvability condition [4]. Simulated patterns have been used to investigate the effects of thermal and chemical undercooling, gravity and fluid convection, and also to promote further insight into the generation of pattern characteristics like tip splitting or sidebranching. Most of the numerical simulations have been initiated from or controlled against experimental observations made with one of the few methods available. Most likely, new experimental techniques can contribute to further qualitative but also quantitative knowledge on dendritic growth.

In metals, equilibrium processes like planar and cellular growth have been investigated by sealed-tube x-ray radiography [6], and later by synchrotron x-ray topography [7], but neither the spatiotemporal resolutions nor the techniques or equipment employed, are adequate for studies of dendritic growth. Sealed-tube x-ray radioscopy has been employed successfully to study stationary segregation phenomena occurring in the liquid phase under alloy solidification in the presence of conductive and convective flows [8].

Information on dendritic growth in metals has been obtained from interrupted processes, either by quenching of the microstructure [9], or by decanting of the melt [10] during the growth. Subsequent metallographic investigations of the microstructures give information on the frozen solid-liquid interface, but the methods are of limited value in analyzing the dynamics of the solidification processes. Certain transparent organic compounds have been used to simulate the solidification of metals [2,11]. These organic materials have low entropies of fusion and therefore solidify like metals in a nonfaceted way, often in hexagonal or cubic crystal systems. The growing crystals of transparent analogs can be studied under a light microscope utilizing the phase contrast at the solid-liquid interface, but none of these analog systems include an opaque alloying element that could display compositional gradients in either of the phases from light absorption differences. In summary, experimental methods that were used in the past are all severely limited with respect to their abilities to evaluate different theoretical models for dendritic growth. This paper reports on a new experimental method where intense and coherent synchrotron x-radiation has been used for *in situ* studies of interfacial and phase-specific spatiotemporal structures which appear during nonequilibrium growth in binary alloys.

Two binary alloys were prepared, with compositions Sn$-$10 wt % Pb and Sn$-$52 wt % Pb, respectively. The alloys were melted and filled into flat rectangular glass containers (cuvettes) made from welding together two 100 μm thick 15×25 mm^2 borosilicate plates, internally spaced by either 0.100(5) or 0.150(5) mm. The cuvette was mounted with its thinnest dimension parallel to the x-ray beam in a sliding device and placed between two furnaces independently adjustable in temperature and

 0031-9007/99/83(24)/5062(4)$15.00

position, enabling control of the temperature gradient, $\partial T/\partial z$, over the sample. A stepper motor was connected to the slider with its axis of translation directed vertically along the spacing between the furnaces.

The experiments were carried out on beam lines ID22 [12] and ID18 [12] at the European Synchrotron Radiation Facility (ESRF). Incident 23.88 or 25 keV monochromatic ($\Delta E/E \sim 10^{-4}$) beams, obtained from filtering undulator harmonics through a vertical double crystal Si_{111} monochromator, were slitted down to a size $\sim 1.0 \times 1.0$ mm^2 about 5 m upstream from the sample. The transverse coherence length at the sample position was typically $\sim 30-80$ μm with a monochromatic flux of the order of 10^{12} photons/(s $\cdot$ mm^2). A fast readout-low noise (FReLoN) CCD camera [13] with a 1024×1024 pixel array, $\sim(19\ \mu\text{m})^2$ pixel size and a 14 bit dynamical range, was used to collect the images. The camera was mounted on an optical microscope head equipped with a $2\times$ magnifying eyepiece, and in addition $10\times$ and $20\times$ magnifying objectives mounted on a motorized support that allowed fine tuning of their focal planes onto a transparent luminescent screen [14]. The screen was a 3.5 μm thick europium-doped lutetium aluminum garnet (LAG:Eu) deposited on a 170 μm yttrium aluminum garnet (YAG) substrate. Including screen and optical aberrations, the maximum resolution of this setup is about 1 μm. An external fast shutter was coupled to the camera triggering. A one-channel readout with storage to disk gave readout/storage-times, t_{rs}, of 0.5 and 0.9 s for 2×2 binned frames and full frames, respectively. A four-channel readout and storage of images directly in computer memory can be used to bring t_{rs} down to ~ 50 ms for a full frame, but this combination was not employed due to technical problems. The software application of the detector also offers online image display.

From a melted sample in thermal contact only with the upper hot furnace, solidification was initiated by lowering the sample cuvette at a constant velocity, $v_{cuv} \in [4.8, 1000]$ μm/s, with nucleation occurring as the cuvette came in thermal contact with the lower furnace operated at temperatures below the alloy solidus. The growth process could now be monitored, collecting consecutive frames at a fixed camera position as the sample was moved further down into the less hot compartment. During the experiments $\partial T/\partial z$ was varied in the range $16.7-150$ K/mm by adjusting the temperatures and the spacing of the furnaces. Exposure times were in the range $0.2-1.0$ s, that together with t_{rs} added up to the total time elapse between consecutive frames. The spatial resolution obtained, in the range $2.5-5$ μm, was determined by the particular combination of readout mode and magnification. In all, 84 separate time series of solidification were collected.

In the solidification studies of Sn–10 wt% Pb we observed columnar dendrites and cellular structures covering a growth velocity of the solid-liquid interface, $v_{sl} \in [10, 600]$ μm/s controlled by varying v_{cuv} and $\partial T/\partial z$. Figure 1 shows a sequence of images of columnar Sn dendrites growing at $v_{sl} \sim 40$ μm/s in a temperature gradient of 19 K/mm. Microsegregation between the dendrite arms can easily be seen as well as a dark, Pb-enriched liquid boundary layer preceding the growing crystal front in a shape presumably determined from liquid diffusion at the interface. The effective spatial resolution in these images was reduced to ~ 5 μm, in order to get sufficiently reliable intensity statistics over the image at 1.0 s exposures. A dark, Pb-rich area can be seen in the lower left section of the images. The extent and shape of this macrosegregated area changes surprisingly fast. The origin of this segregation phenomenon is not known; it may

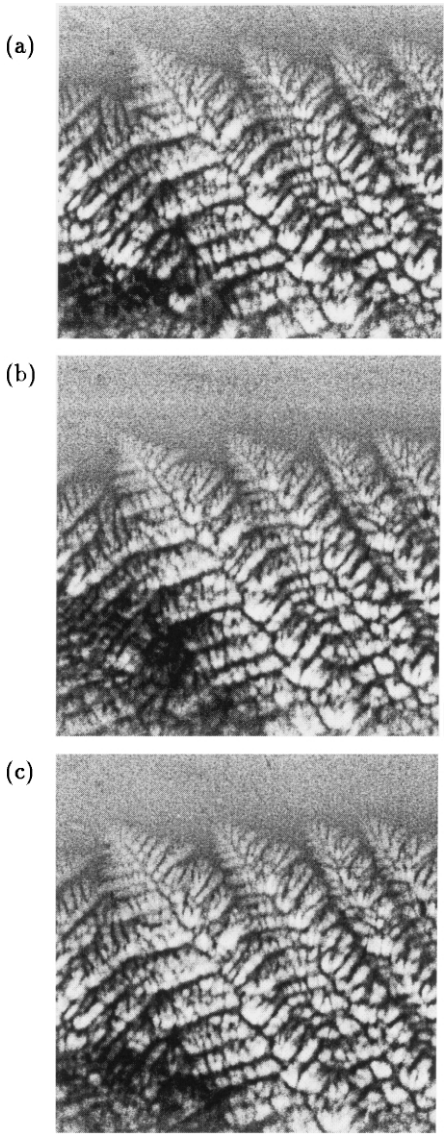

FIG. 1. Columnar dendritic growth of Sn crystals in an Sn–10 wt% Pb alloy. $\partial T/\partial z \sim 19$ K/mm, $v_{cuv} = 9.6$ μm/s, exposure time = 1.0 s, 2×2 binned image, $\sim 1 \times 1$ mm^2 field of view. Sample-detector distance 10 cm. (a) t_0, (b) $t_0 + 1.5$ s, (c) $t_0 + 3.0$ s.

be a consequence of the confined space in which the crystals grow.

Figure 2 shows cellular growth. The temperature gradient has been drastically increased to 150 K/mm as determined from the temperatures and spacing between the furnaces. It can be seen from the series of pictures that the thermal stability is higher; the solidification front growing steadily at a rate $v_{sl} \sim 16\ \mu$m/s. At this high $\partial T/\partial z$ the growth temperature is depressed and crystals with a low alloy composition can survive ahead of the front. A crystal fragment that has been detached from the front can be seen to the right in the images. It attaches to the front and continues to grow as a new crystal. This detachment/crystal multiplication phenomenon is assumed to occur in metals, but has not been observed previously *in situ*.

The other alloy composition, Sn–52 wt% Pb, is well suited for studies of equiaxed growth processes. The eutectic point of the Sn-Pb system is at 38 wt% Pb, thus, in this case, the primary crystals will be Pb. From Figure 3 it can be seen that continuous nucleation takes place in the undercooled melt ahead of the solidification front, but it is not clear whether the nucleation sites occur on the glass or in the liquid. The crystals grow in an equiaxed manner, dendrite arms parallel to the heat flow growing to substantial lengths. A directional

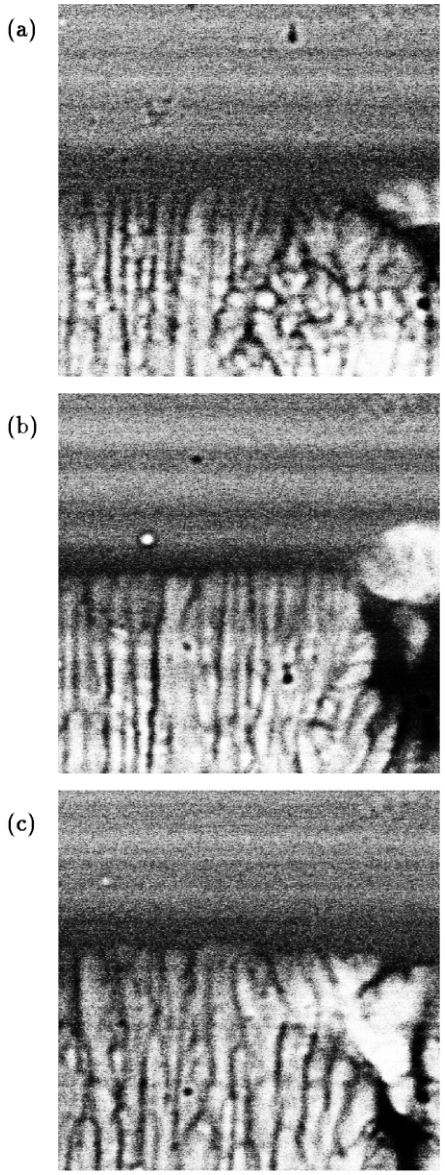

FIG. 2. Cellular growth of Sn crystals in an Sn–10 wt% Pb alloy. $\partial T/\partial z \sim 150$ K/mm, $v_{cuv} = 9.6\ \mu$m/s, exposure time = 0.5 s, 2×2 binned image, $\sim 0.5 \times 0.5$ mm^2 field of view. Sample-detector distance 75 cm. (a) t_0, (b) $t_0 + 31$ s, (c) $t_0 + 62$ s.

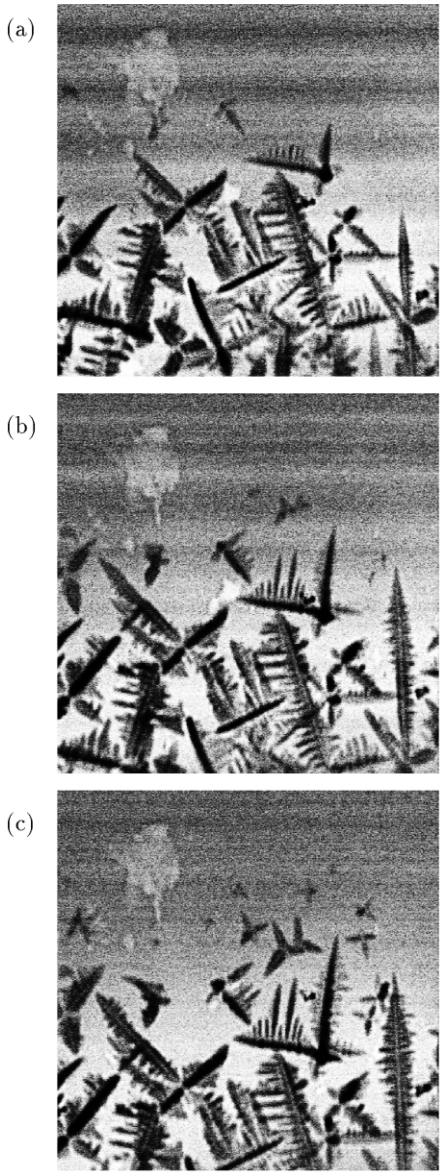

FIG. 3. Equiaxed dendritic growth of Pb crystals in an Sn–52 wt% Pb alloy. $\partial T/\partial z \sim 29.5$ K/mm, $v_{cuv} = 9.6\ \mu$m/s, exposure time = 1.0 s, 2×2 binned image, $\sim 1 \times 1$ mm^2 field of view. Sample-detector distance 75 cm. (a) t_0, (b) $t_0 + 4.5$ s, (c) $t_0 + 9.0$ s.

front cannot develop since new nuclei are formed in the volume preceding the interface—a directional front of pure Pb would also require a strong Sn diffusion since the melt is almost a 50%/50% mixture of the two elements. Equiaxed growth of alloys has not been observed *in situ* with other experimental methods.

The SnPb alloys were selected for these primary studies because of their rather low solidus/liquidus temperatures, and because the system has a well-known phase diagram making SnPb alloys suited for exploratory work. A practical problem with this system is the strong absorption of x rays by Sn and especially by Pb in the energy range ($<$20 keV) where the scintillator has its highest quantum efficiency. The luminescent screen is made as thin as possible to make x-ray to light conversion most likely to occur within the area associated with the focal depth of the objectives, hence optimizing spatial resolution at the expense of quantum efficiency. Photons at 25 keV have less than 25% transmission through the 100 μm Sn–10 wt% Pb alloy which prevents full advantage to be taken of the temporal resolution attainable with the camera and making it necessary also to compromise on spatial resolution.

Experiments with more transparent alloys (e.g., AlCu) with a higher transmission at an energy more optimized for the screen will produce results with the full camera resolutions. Thermocouples introduced into the sample cuvette can be used to map out $\partial T/\partial z$ locally in the area surrounding the progressing interface. With these improvements, results from the method presented here will have spatiotemporal resolutions close to the ones obtainable with transparent analogs, and will in addition contain phase-specific information on solute diffusion and macrosegregation in the solid. We believe this type of experimental output could open for new efforts in numerical simulations and theoretical modeling, and eventually provide new knowledge on dendritic growth in metals.

We thank Mr. K. Ramsøskar, NTNU, for valuable help in constructing and building the sample stage, Dr. D. Fernandez and Dr. J.-C. Labiche, ESRF, for their assistance in setting up the FReLoN camera, and finally the beam line staffs at ID17 and ID18 at ESRF for generous equipment support. NFR is acknowledged for Grant No. 116469/431.

[1] W. Kurz and R. Trivedi, Acta Metall. **38**, 1 (1990).
[2] M. E. Glicksman, R. J. Schaefer, and J. D. Ayers, Metall. Trans. **7A**, 1747 (1976).
[3] J. S. Langer, Phys. Today **45**, No. 10, 24 (1992).
[4] J. S. Langer, Phys. Rev. A **33**, 435 (1986); D. I. Meiron, Phys. Rev. A **33**, 2704 (1986); P. Pelcé and Y. Pomeau, Stud. Appl. Math. **74**, 245 (1986); M. Ben Amar and Y. Pomeau, Europhys. Lett. **2**, 307 (1986); D. Kessler and H. Levine, Phys. Rev. Lett. **57**, 3069 (1986); A. Barbieri, D. C. Hong, and J. S. Langer, Phys. Rev. A **35**, 1802 (1987); D. Bensimon, P. Pelcé, and B. I. Shraiman, J. Phys. (Paris) **48**, 2081 (1987); Y. Saito, G. Goldbeck-Wood, and H. Müller-Krumbhaar, Phys. Rev. A **38**, 2148 (1988); M. Ben Amar and P. Pelcé, Phys. Rev. A **39**, 4263 (1989).
[5] A. Schmidt, J. Comp. Phys. **125**, 293 (1996); A. A. Wheeler, W. J. Boettinger, and G. B. McFadden, Phys. Rev. A **45**, 7424 (1992); G. B. McFadden, A. A. Wheeler, R. J. Braun, S. R. Coriell, and R. F. Sekerka, Phys. Rev. E **48**, 2016 (1993); J. A. Warren and W. J. Boettinger, Acta Metall. **43**, 689 (1995); A. Karma and W.-J. Rappel, Phys. Rev. E **53**, R3017 (1996); S.-L. Wang and R. F. Sekerka, Phys. Rev. E **53**, 3760 (1996); D. Juric and G. Tryggvason, J. Comp. Phys. **123**, 127 (1996); D. Juric, Mater. Res. Soc. Symp. Proc. **538**, 163 (1999); M. D. Kunka, M. R. Foster, and S. Tanveer, Phys. Rev. E **56**, 3068 (1997); **59**, 673 (1999).
[6] M. P. Stephenson and J. Beech, J. Solidification Cast. Met. Conf. Proc. **34** (1977).
[7] T. Matsumiya, W. Yamada, T. Ohashi, and O. Nittono, Metall. Trans. **A18**, 723 (1987); G. Grange, J. Gastaldi, C. Jourdon, and B. Billia, Synchrotron. Radiation News **7**, 12 (1994).
[8] J. N. Koster, R. Derebail, and A. Grotzbach, Appl. Phys. A **64**, 45 (1997); J. N. Koster, J. Mater. **49**, 31 (1997); J. N. Koster, T. Seidel, and R. Derebail, J. Fluid. Mech. **343**, 29 (1997).
[9] A. M. de Figuerdo, Y. Samartha, and M. C. Flemmings, in *Light Metals: Proceedings of the Technical Sessions Presented by the TMS Aluminum Committee at the 127th TMS Annual Meeting, San Antonio, TX, 1998* (TMS, Warrendale, PA, 1998).
[10] F. Weinberg and B. Chalmers, Can. J. Phys. **29**, 382 (1951); F. Weinberg and B. Chalmers, Can. J. Phys. **30**, 488 (1952).
[11] K. Somboonsuk and R. Trivedi, Acta Metall. **33**, 1051 (1985); R. Trivedi and K. Somboonsuk, Acta Metall. **33**, 1061 (1985); M. Muschol, D. Liu, and H. Z. Cummins, Phys. Rev. A **46**, 1038 (1992); J. C. LaCombe, M. B. Koss, V. E. Fradkov, and M. E. Glicksman. Phys. Rev. E **52**, 2778 (1995).
[12] *ESRF Beamline Handbook*, edited by R. Mason (ESRF User Office, Grenoble, France, 1997), 4th ed.
[13] J.-C. Labiche, J. Segura-Puchades, D. van Brusel, and J. P. Moy, ESRF Newslett. **25**, 41 (1996).
[14] A. Koch, C. Raven, P. Spanne, and A. Snigirev, J. Opt. Soc. Am. A **15**, 1940 (1998).